Disorder-induced dynamics in a pair of coupled heterogeneous phase oscillator networks

Carlo R. Laing*
Institute of Information and Mathematical Sciences, Massey University, Private Bag 102-904 NSMC, Auckland, New Zealand.
phone: +64-9-414 0800 extn. 41038 fax: +64-9-4418136
(Dated: October 9, 2012)

We consider a pair of coupled heterogeneous phase oscillator networks and investigate their dynamics in the continuum limit as the intrinsic frequencies of the oscillators are made more and more disparate. The Ott/Antonsen ansatz is used to reduce the system to three ordinary differential equations. We find that most of the interesting dynamics, such as chaotic behaviour, can be understood by analysing a gluing bifurcation of periodic orbits; these orbits can be thought of as "breathing chimeras" in the limit of identical oscillators. We also add Gaussian white noise to the oscillators' dynamics and derive a pair of coupled Fokker-Planck equations describing the dynamics in this case. Comparison with simulations of finite networks of oscillators are used to confirm many of the results.

PACS numbers: 05.45.Xt, 05.45.Ac
Keywords: coupled oscillators, bifurcation, chaos, noise, chimera

The synchronisation of coupled oscillator networks is an ongoing topic of interest. Here we consider a pair of networks of phase oscillators, with all-to-all coupling both within and between networks. When the oscillators are identical, the system is known to support both stationary and "breathing" chimera states, where one population is synchronised while the other is not. We use the degree of heterogeneity of the oscillators as a parameter, and by varying it we investigate the new dynamics induced by this "frozen" disorder. We find that for sufficiently high disorder, the differential equations governing the dynamics of the macroscopic order parameters of the network show chaotic behaviour. This chaotic behaviour is the result of a gluing bifurcation involving a saddle fixed point in a three-dimensional phase space. We also consider adding Gaussian white noise to the oscillator dynamics and show that this "temporal" disorder can have surprising effects on the network dynamics.

I. INTRODUCTION

The behaviour of large collections of interacting "units" has long been of interest [1]. One commonly-studied example is that of coupled oscillator networks, where each unit in isolation is capable of oscillating and the collective dynamics are of interest [2, 3]. The dynamics of a moderate number of non-identical oscillators may be quite complex [4, 5], but one productive approach for this type of problem is to take the continuum limit of an infinite number of oscillators and derive a dynamical equation governing the evolution of the probability density function describing the state of the network [6, 7]. This approach has been particularly successful for networks of phase oscillators, where the state of each oscillator is described by a single angular variable [8–11]. Of course, the relationship between the behaviour in the continuum limit and that of a finite network should be carefully considered [12].

One question of interest in the study of coupled phase oscillator networks is whether or not chaotic behaviour can occur in the continuum limit. In finite networks several authors have numerically found evidence for chaotic behaviour [4, 13, 14], but in all cases the most positive Lyapunov exponent decayed to zero as the size of the network increased. This question was recently addressed by So and Barreto [15], who considered an infinite network of coupled phase oscillators whose intrinsic frequencies were drawn from a particular bimodal distribution, and which was periodically forced. These authors used the recent ansatz of Ott and Antonsen [16–18] to reduce the infinite system to two coupled, complex, non-autonomous ordinary differential equations (ODEs). By assuming that the two complex variables had equal magnitude, and examining only the difference in phases between the variables, they reduced this system to a pair of coupled, real, non-autonomous ODEs. Building on the analysis of the autonomous case [19] they then numerically showed that this pair of equations exhibited chaotic behaviour. However, they did not discuss the relationship between this "macroscopic" chaos and the dynamics of a finite network at the same parameter values. They gave only a heuristic explanation of the origin of the chaotic behaviour in terms of "moving targets", and conjectured that either periodic forcing or the presence of a "slow" variable would be necessary in order to observe macroscopic chaos in a network of coupled phase oscillators.

*Electronic address: c.r.laing@massey.ac.nz

One of the results of this paper is to show that macroscopic chaos can occur in an infinite network consisting of a pair of coupled heterogeneous networks of phase oscillators. Neither periodic forcing nor the presence of a slow variable are required, and we show that the chaotic behaviour is associated with a symmetric "gluing" bifurcation, which has been analysed previously in different contexts [20–22]. This result is part of the general analysis of this network, where the degree of heterogeneity in the network is a key parameter. Specifically, we show that the network must be sufficiently heterogeneous for this chaotic behaviour to occur.

The structure of the paper is as follows: in Sec. II we present the equations describing a finite network of coupled phase oscillators and their reduced description obtained in the continuum limit using the ansatz of Ott and Antonsen. Section III gives the results of analysing those reduced equations in both the small heterogeneity regime and the large heterogeneity regime. We also discuss the relationship between the macroscopic chaos seen and the dynamics of a finite network. In Sec. IV we consider adding Gaussian white noise to the oscillator dynamics, as another form of disorder, and briefly analyse the resulting coupled Fokker-Planck equations. We use the strength of noise as a parameter and show that the behaviour predicted by these Fokker-Planck equations also occurs in finite networks of oscillators. We conclude in Sec. V.

II. MODEL EQUATIONS

The equations describing the finite network of $2N$ phase oscillators that we will consider are

$$\begin{aligned}\frac{d\theta_i^1}{dt} &= \omega_i^1 + \frac{\mu}{N}\sum_{j=1}^{N}\sin\left(\theta_j^1-\theta_i^1-\alpha\right)\\ &+ \frac{\nu}{N}\sum_{j=1}^{N}\sin\left(\theta_j^2-\theta_i^1-\alpha\right) \qquad (1)\\ \frac{d\theta_i^2}{dt} &= \omega_i^2 + \frac{\mu}{N}\sum_{j=1}^{N}\sin\left(\theta_j^2-\theta_i^2-\alpha\right)\\ &+ \frac{\nu}{N}\sum_{j=1}^{N}\sin\left(\theta_j^1-\theta_i^2-\alpha\right) \qquad (2)\end{aligned}$$

for $i = 1, \dots N$, where the superscript indicates to which of two populations an oscillator belongs, μ and ν are given by $\mu = (1+A)/2$ and $\nu = (1-A)/2$ where A is a positive parameter, $\alpha \in (0, 2\pi)$ is a constant, and the intrinsic frequencies $\omega_i^{1,2}$ are all chosen randomly from a distribution $g(\omega)$. This system was previously studied by Abrams et al. [9] for the case that $g(\omega) = \delta(\omega)$, i.e. identical oscillators, and by Laing [23] and Montbrió et al. [24] for the case that $g(\omega)$ was a Lorentzian. A more general system of this form was considered by Barreto et al. [25]. This pair of networks can be thought of as the simplest form of a "network of networks" [26]. Alternatively, it can be regarded as the simplest form of network with "non-local" coupling [27–29]: there is all-to-all "local" coupling of strength μ within a population and all-to-all "non-local" coupling of strength ν between populations. Note that a system of discrete chemical oscillators conceptually equivalent to (1)-(2) has recently been studied [30], and that several electrical systems of importance can be described by coupled oscillator networks of this form [31, 32]. Also, recent experiments in an optical system have shown the existence of "chimera" states similar to those discussed in this paper [33].

The ansatz of Ott and Antonsen [16–18] has proved very useful in the study of infinite networks of sinusoidally-coupled phase oscillators such as (1)-(2) [15, 19, 34–43]. The ansatz is essentially an assumption on the form of the Fourier series describing the angular dependence of the probability density function; it allows one to derive exact dynamical equations for macroscopic, order-parameter-like variables, which are valid on an attracting invariant manifold. The ansatz applies to infinite networks of heterogeneous phase oscillators (although see [44, 45] for an application to an infinite ensemble of finite-size networks), and simplifies the analysis of such systems by effectively removing one of the variables from the continuity equation governing the evolution of the probability density function.

Under the assumption that $g(\omega)$ is a Lorentzian centred at $\omega = \Omega$, i.e.

$$g(\omega) = \frac{D/\pi}{(\omega-\Omega)^2 + D^2} \qquad (3)$$

where D is a measure of the width of g, and in the limit $N \to \infty$, the Ott/Antonsen ansatz [16–18] allows one to show that the order parameters describing the network (1)-(2) satisfy the complex ODEs

$$\begin{aligned}\frac{dz_1}{dt} &= -(D+i\Omega)z_1 + (e^{-i\alpha}/2)(\mu z_1 + \nu z_2)\\ &- (e^{i\alpha}/2)(\mu\overline{z}_1 + \nu\overline{z}_2)z_1^2 \qquad (4)\\ \frac{dz_2}{dt} &= -(D+i\Omega)z_2 + (e^{-i\alpha}/2)(\mu z_2 + \nu z_1)\\ &- (e^{i\alpha}/2)(\mu\overline{z}_2 + \nu\overline{z}_1)z_2^2 \qquad (5)\end{aligned}$$

where the order parameters [8, 46] are given by

$$z_k(t) = \lim_{N\to\infty}\frac{1}{N}\sum_{j=1}^{N}\exp\left(i\theta_j^k\right) \qquad (6)$$

for $k = 1, 2$. The derivation of these equations is given in [23] and similar ideas are used in [9, 10, 19], so we do not repeat the derivation here. Note that the magnitude of the order parameter z_k is a measure of the degree of synchrony within population k.

Writing $z_1 = r_1 e^{-i\phi_1}$ and $z_2 = r_2 e^{-i\phi_2}$ and defining

$\phi = \phi_1 - \phi_2$, (4)-(5) can be written as

$$\frac{dr_1}{dt} = -Dr_1 + \left(\frac{1-r_1^2}{2}\right)\left[\mu r_1 \cos\alpha + \nu r_2 \cos(\phi - \alpha)\right] \quad (7)$$

$$\frac{dr_2}{dt} = -Dr_2 + \left(\frac{1-r_2^2}{2}\right)\left[\mu r_2 \cos\alpha + \nu r_1 \cos(\phi + \alpha)\right] \quad (8)$$

$$\frac{d\phi}{dt} = \left(\frac{r_1^2+1}{2r_1}\right)\left[\mu r_1 \sin\alpha - \nu r_2 \sin(\phi - \alpha)\right] - \left(\frac{r_2^2+1}{2r_2}\right)\left[\mu r_2 \sin\alpha + \nu r_1 \sin(\phi + \alpha)\right] \quad (9)$$

Note that Ω (the mean of the intrinsic frequencies) does not appear in these equations. The case when $D = 0$ (identical oscillators) was studied by Abrams et al. [9]. They noted that in this case, $r_1 = 1$ defines an invariant manifold; they then analysed the resulting pair of ODEs for r_2 and ϕ. Their interest was in "chimera" states, in which one population is synchronised (population 1 in this case, as $r_1 = 1$) and the other is not (i.e. $r_2 \neq 1$). They found that for α less than but sufficiently close to $\pi/2$, increasing A lead to the creation of two chimera states through a saddle-node bifurcation, one of which went unstable through a supercitical Hopf bifurcation as A was increased further, leading to a "breathing" chimera state. This was destroyed in a homoclinic bifurcation as A increased yet further. Their results are shown in Fig. 4 of Abrams et al. [9], where $\beta = \pi/2 - \alpha$. Note that these authors did not show that $r_1 = 1$ was an attracting manifold, only that it was invariant.

A partial analysis of (7)-(9) was given by Laing [23], with concentration on the effects of increasing D for fixed A and α, and determining the fate of chimera states. In this paper we fix $\alpha = \pi/2 - 0.05$ and consider in much greater detail the effects of varying A and D. We are interested in not only whether chimera states are robust to heterogeneity, i.e. increasing D (they are [23]) but what other dynamics can occur as the networks are made more heterogeneous. For example, can chaotic dynamics occur, and if so what is the mechanism for their creation?

III. RESULTS

We now show the results of analysing (7)-(9) in two regimes: $0 \leq D \leq 0.001$ (small D) and $0.001 < D \leq 0.01$ (large D). Recall that we fix $\alpha = \pi/2 - 0.05$ and that $\mu = (1+A)/2$ and $\nu = (1-A)/2$. Firstly, note that (7)-(9) are invariant under the transformation $\Sigma : (r_1, r_2, \phi) \mapsto (r_2, r_1, -\phi)$, corresponding to an interchange of the two oscillator populations. Clearly, the origin is always a fixed point, (which we will not consider from now on) and there exists another fixed point that we will call S, which is fixed by Σ. The coordinates of S are given by $(r_1, r_2, \phi) = (\sqrt{1 - 2D/\cos\alpha}, \sqrt{1 - 2D/\cos\alpha}, 0)$; this fixed point exists for $0 \leq D < (\cos\alpha)/2 \approx 0.025$.

All numerical results were obtained using Matlab [47] and most numerical integration was performed using `ode45` with default settings. Local bifurcations were followed using pseudo-arclength continuation, and global bifurcations were found manually by sweeping through parameter space. Simulations such as those shown in Fig. 4 took several seconds, while Fig. 7 took many hours of computation. Equations (20)-(21) are time-consuming to simulate due to the powers of n on their right-hand sides.

A. Small Heterogeneity

The results of following the fixed points of (7)-(9) and the resulting bifurcations are shown in Fig. 1. We start by discussing the limit of $D = 0$, as studied by Abrams et al. [9]. They used the Ott/Antonsen ansatz to derive (4)-(5), but it was later shown that the manifold described by this ansatz was *attracting* only when *non-identical* oscillators were used, i.e. when $D > 0$ [16]. (The manifold is invariant for all D.) Instead, the dynamics for $D = 0$ are described by using the Watanabe/Strogatz ansatz [48], and Pikovsky and Rosenblum [49] showed that the network (1)-(2) could undergo more complicated dynamics than those found by Abrams et al. [9] (for $D = 0$). In our analysis of (7)-(9) we varied D from positive to negative and found that the intersection of bifurcation curves with the line $D = 0$ were consistent with those found by Abrams et al. [9]: we see a saddle-node bifurcation, then a Hopf, then a homoclinic, as A is increased. These bifurcations are all generic and codimension-one, so in (D, A) parameter space we expect curves on which they occur, with these curves leading away from the A-axis, and that is what is observed. However, other interesting behaviour occurs as D is increased. We now describe Fig. 1 in detail.

In region a, the only invariant set of interest is the fixed point S, which is stable. As we cross from region a to region b, two pairs of symmetrically related fixed points are created in saddle-node bifurcations. These points are labelled $P_1^{\pm}$ (P_1^+ is stable and P_1^- is a saddle) and $P_2^{\pm}$. The transformation Σ takes P_1^+ to P_2^+ and similarly for P_1^- and P_2^-. As we cross from region b to region c, both P_1^+ and P_2^+ undergo supercritical Hopf bifurcations, creating periodic orbits Γ_1 and Γ_2, which are mapped to one another by Σ (see Fig. 2, top). Crossing from region c to region d, Γ_1 and Γ_2 collide with P_1^- and P_2^-, respectively, in a homoclinic bifurcation. In region d the only attractor is fixed point S. Crossing from region b to region h, P_1^- and P_2^- collide with S in a subcritical pitchfork bifurcation, making S a saddle in region h. Crossing from region h to region g, both P_1^+ and P_2^+ undergo supercritical Hopf bifurcations, creating the periodic orbits that we have called Γ_1 and Γ_2. Crossing from region g to region f, both Γ_1 and Γ_2 collide with S in a gluing bifurcation [50],

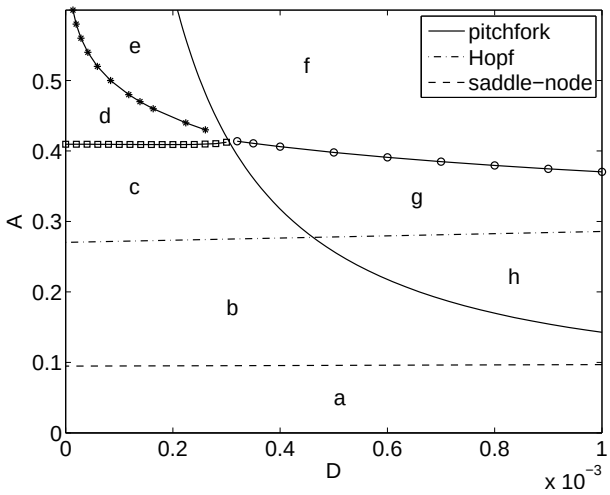

FIG. 1: Bifurcation set of (7)-(9) for small heterogeneity. Curves of the three local bifurcations are labelled in the Figure. Squares: homoclinic bifurcation of P_1^- and P_2^-, destroying Γ_1 and Γ_2. Circles: symmetric homoclinic connection to S, gluing Γ_1 and Γ_2 together to form Π. Stars: symmetric heteroclinic bifurcation of P_1^- and P_2^-, destroying Π.

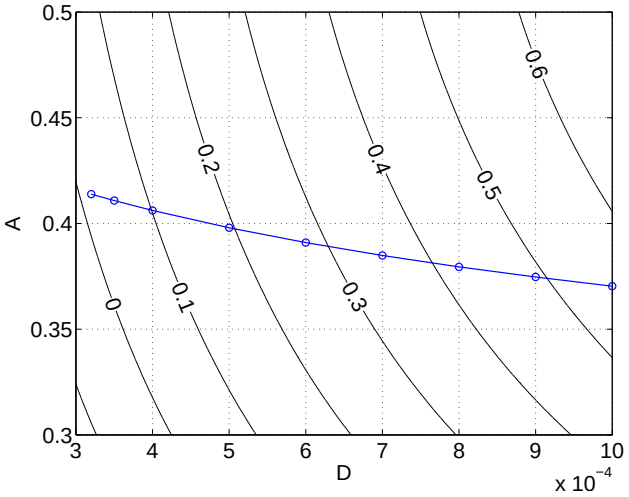

FIG. 3: Circles joined by lines: the gluing bifurcation shown in Fig. 1. Solid lines are contours of equal values of the saddle index for S, $\delta = \lambda_1/|\lambda_2|$, where the eigenvalues of the Jacobian at S are $\lambda_3 < \lambda_2 < 0 < \lambda_1$. Note that the zero contour corresponds to the pitchfork bifurcation curve shown in Fig. 1.

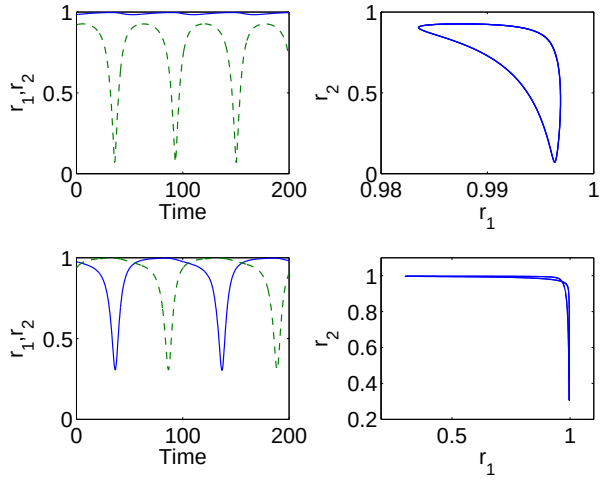

FIG. 2: Typical examples of the periodic orbits Γ_1 (top, when $A = 0.35$) and Π (bottom, when $A = 0.5$). The left column shows time series of r_1 (solid) and r_2 (dashed) and the right panels show orbits in the (r_1, r_2) plane. Other parameters: $D = 0.0005$.

which creates a stable "period-two" orbit which we label Π, mapped to itself under Σ (see Fig. 2, bottom), which exists in region f. Crossing from region f to region e, S undergoes a subcritical pitchfork bifurcation, creating P_1^- and P_2^-, and becoming stable. Crossing from region e to region d, the periodic orbit Π is involved in a symmetric heteroclinic bifurcation (destroying Π), where the unstable manifold of P_1^- intersects the stable manifold of P_2^- and vice versa. There is bistability in regions b,c and e.

There is one codimension-two point in Fig. 1, where the curves of homoclinic and heteroclinic bifurcations intersect the curve on which S undergoes a pitchfork bifurcation. The unfolding of this pitchfork-homoclinic bifurcation is given in Deng [51] and our results are consistent with that analysis. We note that on the curve of homoclinic bifurcations separating regions c and d, the destruction of the stable periodic orbits Γ_1 and Γ_2 is consistent with the saddle indices of P_1^- and P_2^- being less than one [21, 52], where the saddle index is defined to be $\delta = \lambda_1/|\lambda_2|$, and the eigenvalues associated with P_1^- (and P_2^-) are $\lambda_3 < \lambda_2 < 0 < \lambda_1$. Also, along the gluing bifurcation separating regions f and g, the saddle index of the fixed point S is less than one, as shown in Fig. 3. Such a bifurcation is discussed in [20–22] and it is known that for $\delta < 1$, the gluing bifurcation corresponds to the destruction of the two stable periodic orbits Γ_1 and Γ_2 and their replacement by the stable periodic orbit Π.

The main effects of increasing D that we have seen are the conversion of the symmetric fixed point S from stable to unstable through a pitchfork bifurcation, and the creation of the periodic orbit Π, which is invariant under Σ, through either a gluing bifurcation or a symmetric heteroclinic bifurcation. On the orbit Π the oscillator populations take turns being nearly synchronous (when the corresponding order parameter has magnitude close to one). When one population is nearly synchronous the other is largely asynchronous, with small order parameter (see Fig. 2 (bottom) and Fig. 4 (bottom)).

We have verified that the different types of behaviour predicted by Fig. 1 for an infinite network actually occur in a finite network of phase oscillators. Figure 4 shows the behaviour of a network of $2N = 600$ oscillators governed by (1)-(2) when $D = 7 \times 10^{-4}$ and $A = 0.05, 0.15, 0.35, 0.45$. The top panel shows the stable

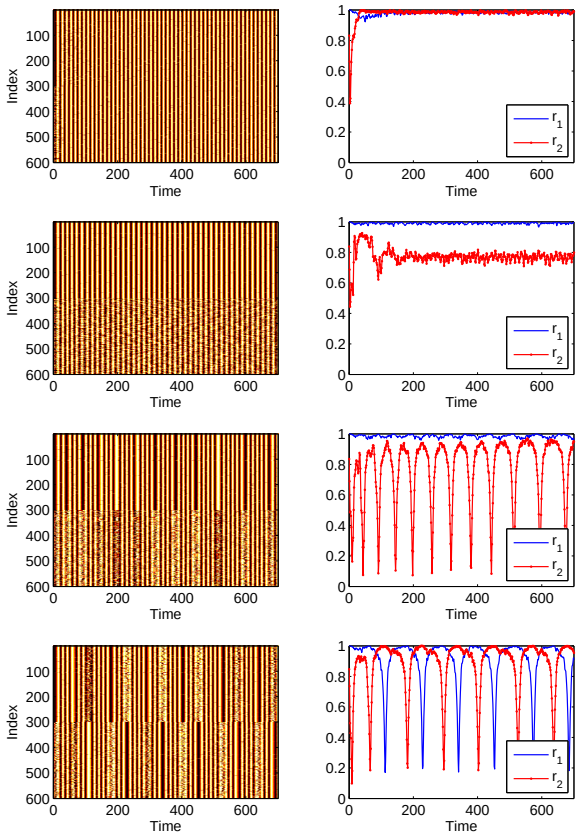

FIG. 4: Dynamics of the phase oscillator network (1)-(2) for $N = 300$ at (top to bottom) $A = 0.05, 0.15, 0.35, 0.45$, when $D = 0.0007$. Left panels show $\sin\theta_i$, colour-coded; right panels show r_1 and r_2, where $r_1 = |(1/300)\sum_{j=1}^{300}\exp(i\theta_j)|$ and $r_2 = |(1/300)\sum_{j=301}^{600}\exp(i\theta_j)|$. Parameters: $\Omega = 0.5$.

fixed point S, the second shows one of the stable states P_1^+/P_2^+, the third panel from the top shows one of the periodic orbits Γ_1/Γ_2, and the bottom panel shows the symmetric periodic orbit Π.

B. Large Heterogeneity

We now consider larger values of D. There are four bifurcation curves which reach the right side of Fig. 1. We want to know where they go as D is increased further, and whether any more interesting dynamics occur. A partial bifurcation set for (7)-(9) is shown in Fig. 5. There are three codimension-2 bifurcation points: the first at $(D, A) \approx (2.5 \times 10^{-3}, 0.1)$, where the pitchfork bifurcation changes from subcritical (for small D) to supercritical (for large D) resulting in the termination of the curve of saddle-node bifurcations. The second occurs at $(D, A) \approx (9 \times 10^{-3}, 0.43)$, where the Hopf bifurcation which creates Γ_1 and Γ_2 changes from supercitical (for small D) to subcritical (for large D), resulting in the termination of a curve of saddle-node bifurcations of the periodic orbits Γ_1 and Γ_2. The third point occurs

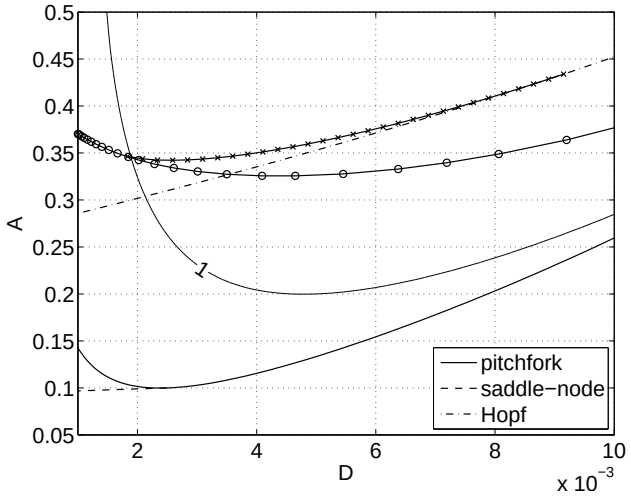

FIG. 5: Bifurcation set of (7)-(9) for $0.001 \le D \le 0.01$. Curves of the three local bifurcations are labelled in the Figure. Circles: symmetric homoclinic connection to S, gluing Γ_1 and Γ_2 together. Crosses: saddle-node bifurcation of the periodic orbit Γ_1 (and of Γ_2.) The thin line labelled "1" is the curve on which the saddle index changes from less than 1 (below the curve) to greater than 1 (above the curve).

at $(D, A) \approx (1.8 \times 10^{-3}, 0.35)$, where the saddle index of the fixed point S involved in the gluing bifurcation changes from less than one (for small D) to greater than one (for large D). Associated with this is the start of a curve of saddle-node bifurcations of periodic orbits (in this case, Γ_1 and Γ_2) which exists in the region $\delta > 1$. From the analysis in [20–22] we also expect the creation of a chaotic attractor when $\delta > 1$, in the vicinity of the gluing bifurcation.

As a first step towards understanding this possible chaotic behavior we show in Fig. 6 several parameter sweeps of (7)-(9) when $D = 4 \times 10^{-3}$, plotting both the values of r_1 when r_2 increases through 0.5 (during a long simulation and after transients have died out) and the most positive Lyapunov exponent. In the top two panels of Fig. 6 A was slowly decreased stepwise, with the initial condition for each new value of A being the final state from the previous simulation. In the bottom two panels of Fig. 6 A was increased stepwise rather than decreased. This technique may help in the detection of multistability. We see evidence of chaotic behaviour, and bistability (for example, when $0.345 < A < 0.35$). Sweeping through both A and D we obtain Fig. 7, which shows the most positive Lyapunov exponent at each point in the parameter plane. At each point one simulation with intial condition $(r_1, r_2, \phi) = (1, 0.6, 0.1)$ was used to calculate the exponent, so any bistability will not be detected. We see that the chaotic region is indeed associated with the point at which the saddle index of the fixed point involved in the gluing bifurcation (S) passes through 1, as predicted [20].

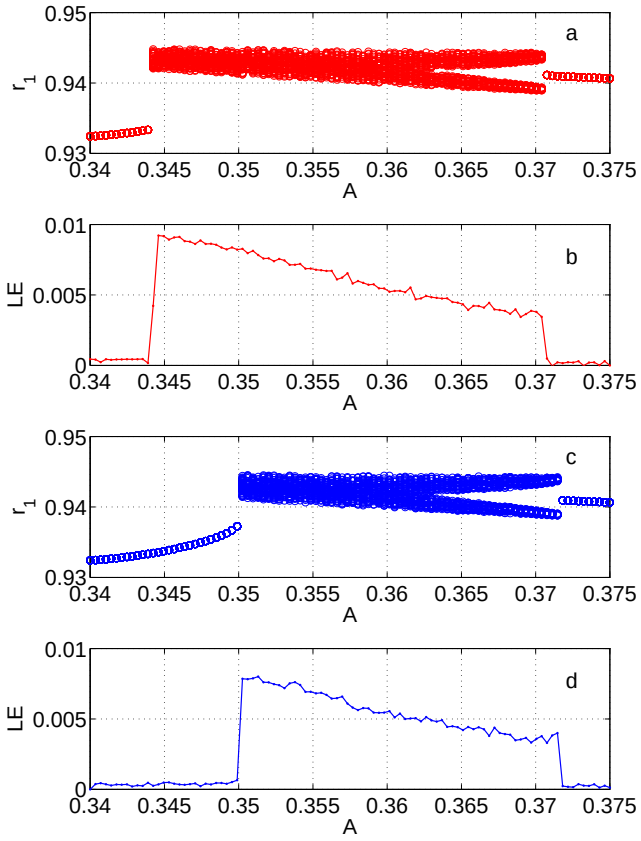

FIG. 6: Parameter sweeps of (7)-(9) for A decreasing (panels a and b) and increasing (c and d), when $D = 4\times10^{-3}$. Panels a and c show the value of r_1 when r_2 increases through 0.5 during a long simulation and after transients have died out. Panels b and d show the most positive Lyapunov exponent of the solution.

C. Results for a finite network

An interesting question involves whether or not the chaotic behaviour observed in the macroscopic description of the infinite network of oscillators (i.e. (7)-(9)) is actually manifested in a finite network of oscillators (i.e. (1)-(2)). As mentioned, a number of authors have numerically found evidence for chaotic behaviour in finite networks of phase oscillators [4, 13, 14], but in all cases the most positive Lyapunov exponent decayed to zero as the size of the network increased. So and Barreto [15] found macroscopic chaos in an infinite network of phase oscillators but did not consider the relationship between this chaotic behaviour and the dynamics of a finite network at the same parameter values.

Figure 8 shows the largest Lyapunov exponent as a function of A for a network of $2N = 200$ oscillators with $D = 0.004$. Referring to Fig. 6 we see that (in the limit of $N \to \infty$) there should be chaotic behaviour over approximately $0.345 < A < 0.37$. However, for the parameter values shown in Fig. 8 the finite network always has a positive Lyapunov exponent, and in the region where the

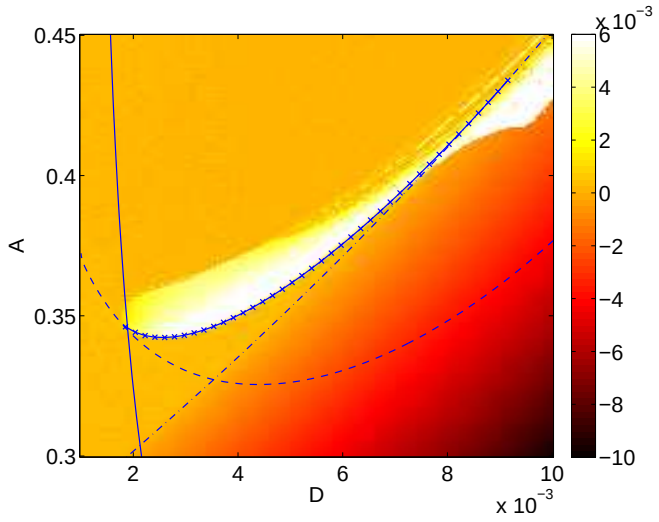

FIG. 7: Largest Lyapunov exponent for (7)-(9) as a function of D and A. Other curves are: dashed: gluing bifurcation; solid: $\delta = 1$; dash-dotted: Hopf; crosses joined by lines: saddle-node bifurcation of periodic orbits. Compare with Fig. 5.

macroscopic model (7)-(9) shows chaotic behavior with maximal exponent on the order of 0.01, the finite network has a maximal exponent larger than that. Thus the transition of the largest Lyapunov exponent from zero to positive and back to zero seen in Fig. 6 is not observed in this finite network. This discrepancy is not a failure of the Ott/Antonsen ansatz, which is valid only in the limit $N \to \infty$. Instead it reflects one of the differences between a finite and an infinite network, which we now explore a little further.

Figures 9 and 10 show the state of the finite network and the full Lyapunov spectrum (calculated using the algorithm of Greene and Kim [53]) at $A = 0.15$ and $A = 0.4$, respectively (c.f. Fig. 8). Similar to the observations of Wolfrum et al. [13] we see that a significant fraction of the Lyapunov exponents are positive, i.e. the system is hyperchaotic. It may be the case that as $N \to \infty$ the most positive exponent will tend to zero, and Fig. 8 will limit to Fig. 6 over the relevant parameter range, but investigating this is computationally challenging and we will not pursue this here. We note that (1)-(2) will always have an exponent of zero, due to the invariance of the system under the application of a constant phase shift to all oscillators, whereas (7)-(9) may have all three exponents negative (at a stable fixed point). Thus we conclude that for these parameter values, the transition to chaotic behaviour in the reduced description (7)-(9) does not necessarily have any implication for the dynamics of the finite network (1)-(2), which may well be (weakly) chaotic over a large range of parameter values.

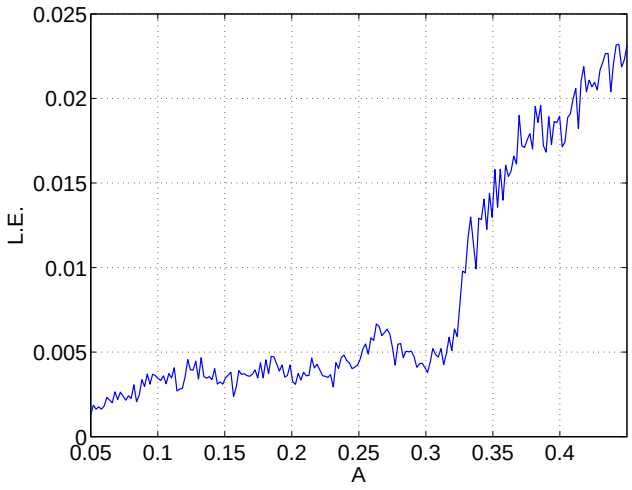

FIG. 8: The largest Lyapunov exponent for the network (1)-(2) with $N = 100$ and $D = 0.004$.

IV. NOISE

We now consider the effects of including temporal disorder, i.e. noise, on the dynamics of the oscillator network (1)-(2). Specifically, we drive the system with Gaussian white noise, replacing (1)-(2) by

$$\frac{d\theta_i^1}{dt} = \omega_i^1 + \frac{\mu}{N}\sum_{j=1}^{N}\sin\left(\theta_j^1 - \theta_i^1 - \alpha\right) + \frac{\nu}{N}\sum_{j=1}^{N}\sin\left(\theta_j^2 - \theta_i^1 - \alpha\right) + \sqrt{2\sigma}\eta_i^1(t) \quad (10)$$

$$\frac{d\theta_i^2}{dt} = \omega_i^2 + \frac{\mu}{N}\sum_{j=1}^{N}\sin\left(\theta_j^2 - \theta_i^2 - \alpha\right) + \frac{\nu}{N}\sum_{j=1}^{N}\sin\left(\theta_j^1 - \theta_i^2 - \alpha\right) + \sqrt{2\sigma}\eta_i^2(t) \quad (11)$$

where each $\eta_i^k(t)$ $(k = 1, 2)$ is a Gaussian white noise with

$$\langle \eta_i^k(t)\rangle = 0 \qquad \langle \eta_i^k(t)\eta_i^k(t')\rangle = \delta(t - t') \quad (12)$$

and σ is the noise intensity [54], where the angled brackets indicate averaging over realisations of the noise. In the limit $N \to \infty$ the system is described by two probability density functions, $f_1(\theta, \omega, t)$ and $f_2(\theta, \omega, t)$, [9, 23] which satisfy the coupled Fokker-Planck equations [55]

$$\frac{\partial f_1}{\partial t} = -\frac{\partial}{\partial\theta}(f_1 v_1) + \sigma\frac{\partial^2 f_1}{\partial\theta^2} \quad (13)$$

$$\frac{\partial f_2}{\partial t} = -\frac{\partial}{\partial\theta}(f_2 v_2) + \sigma\frac{\partial^2 f_2}{\partial\theta^2} \quad (14)$$

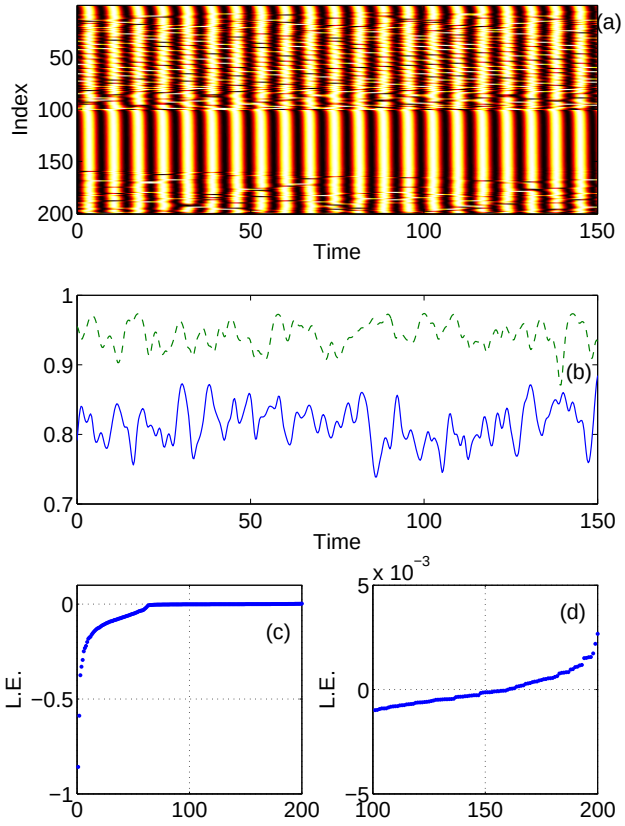

FIG. 9: (a): behaviour of the network (1)-(2) at $A = 0.15$ ($\sin\theta$ is shown colour-coded). (b): r_1 (solid blue) and r_2 (dashed green) as functions of time for the state in the top panel, where $r_1 = |(1/100)\sum_{j=1}^{100}\exp(i\theta_j)|$ and $r_2 = |(1/100)\sum_{j=101}^{200}\exp(i\theta_j)|$. (c)-(d): Lyapunov spectrum, i.e. all $2N$ Lyapunov exponents, for the state shown here. [(d) is an enlargement of the rightmost part of (c).] Parameters: $N = 100, D = 0.004$.

where

$$v_1 = \omega + \frac{1}{2i}\left[e^{-i(\theta+\alpha)}(\mu z_1 + \nu z_2) - e^{i(\theta+\alpha)}(\mu\overline{z}_1 + \nu\overline{z}_2)\right] \quad (15)$$

$$v_2 = \omega + \frac{1}{2i}\left[e^{-i(\theta+\alpha)}(\mu z_2 + \nu z_1) - e^{i(\theta+\alpha)}(\mu\overline{z}_2 + \nu\overline{z}_1)\right] \quad (16)$$

and

$$z_k(t) = \int_0^{2\pi}\int_{-\infty}^{\infty} e^{i\theta} f_k(\theta, \omega, t)\, d\omega\, d\theta \quad (17)$$

for $k = 1, 2$. Recall that ω is a continuous variable with distribution (3). The mean of the intrinsic frequencies, Ω, can be set to zero by going to a rotating coordinate frame, so we do that here. Writing the f_k as Fourier

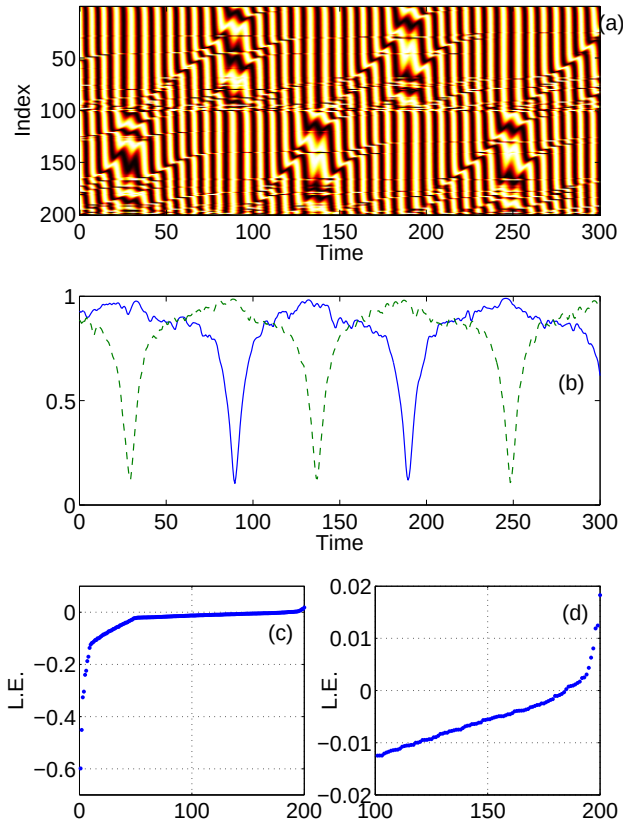

FIG. 10: (a): behaviour of the network (1)-(2) at $A = 0.4$ ($\sin\theta$ is shown colour-coded). (b): r_1 (solid blue) and r_2 (dashed green) as functions of time for the state in the top panel, where $r_1 = |(1/100)\sum_{j=1}^{100}\exp(i\theta_j)|$ and $r_2 = |(1/100)\sum_{j=101}^{200}\exp(i\theta_j)|$. (c)-(d): Lyapunov spectrum, i.e. all $2N$ Lyapunov exponents, for the state shown here. [(d) is an enlargement of the rightmost part of (c).] Parameters: $N = 100, D = 0.004$.

series in θ:

$$f_1(\theta,\omega,t) = \frac{g(\omega)}{2\pi}\left[1+\sum_{n=1}^{\infty}A_n(\omega,t)e^{in\theta}+c.c.\right] \quad (18)$$

$$f_2(\theta,\omega,t) = \frac{g(\omega)}{2\pi}\left[1+\sum_{n=1}^{\infty}B_n(\omega,t)e^{in\theta}+c.c.\right] \quad (19)$$

where "*c.c.*" is the complex conjugate of the previous term, we obtain the following ODEs:

$$\frac{da_n}{dt} = -n\left\{Da_n+\sigma na_n+\left[e^{-i\alpha}(\mu\overline{a}_1+\nu\overline{b}_1)a_{n+1} - e^{i\alpha}(\mu a_1+\nu b_1)a_{n-1}\right]/2\right\} \quad (20)$$

$$\frac{db_n}{dt} = -n\left\{Db_n+\sigma nb_n+\left[e^{-i\alpha}(\mu\overline{b}_1+\nu\overline{a}_1)b_{n+1} - e^{i\alpha}(\mu b_1+\nu a_1)b_{n-1}\right]/2\right\} \quad (21)$$

for $n = 1, 2, \ldots$, where $a_0 = b_0 = 1$, $a_k(t) = A_k(-iD,t)$, and $b_k(t) = B_k(-iD,t)$. We have used residue theory and the specific form of $g(\omega)$ to perform the integral over ω in (17) [18, 23]. Note that when $\sigma = 0$, the Ott/Antonsen ansatz $a_n(t) = [a(t)]^n$ and $b_n(t) = [b(t)]^n$ reduces the infinite set of equations (20)-(21) to the pair of complex ODES (4)-(5), where $z_1 = \overline{a}$ and $z_2 = \overline{b}$.

To demonstrate the effects of temporal noise alone we set $D = 0$ (i.e. use identical oscillators), fix $A = 0.37$ and $\alpha = \pi/2 - 0.05$ and consider several different values of σ. Figure 11 shows, in the left column, solutions of (20)-(21) for $\sigma = 0.00003, 0.0003$ and 0.01 (top to bottom). (We truncate (20)-(21) at $n = 200$ and set $a_{201} = b_{201} = 0$.) Referring back to Fig. 1 (and under the assumption that the dynamics seen for $D = 0$ are robust and persist for small noise, as they do for small D) we see that for σ sufficiently small, one of the attractors at these parameter values should be the "breathing chimera" in which one order parameter undergoes large oscillations while the other undergoes small oscillations about 1. (This state is analogous to the periodic orbit Γ_1 (or Γ_2) seen in Fig. 2, top.) This is indeed seen in Fig. 11 (top left). As σ is increased, Fig. 11 shows that this periodic orbit seems to undergo a gluing bifurcation, resulting in the stable periodic solution mapped to itself under Σ shown in Fig. 11, middle left. A further increase in σ results in a stable fixed point on which $|a_n| = |b_n|$ for all n (Fig. 11, bottom left).

To check these results we show in the right column of Fig. 11 the results of simulating (10)-(11) with the same parameter values as those in the left column for a network with $N = 1000$. The agreement is very good and gets better as N is increased (not shown). We conclude this short section by noting that the addition of Gaussian white noise to the oscillator dynamics can have significant, non-trivial effects, and that these can be studied using a finite-dimensional approximation to the coupled Fokker-Planck equations (13)-(14).

V. CONCLUSION

We have considered a simple network formed by coupling two subnetworks of heterogeneous phase oscillators. The ansatz of Ott and Antonsen was used to derive three ODEs which governed the dynamics of our network in the limit of an infinite number of oscillators, and a Lorentzian frequency distribution. The study of these ODEs as the spread of the oscillators' intrinsic frequencies was increased revealed several bifurcations leading to oscillations in which the two subnetworks periodically alternate in levels of synchrony (a pattern not seen when the oscillators are sufficiently similar), and to chaotic behaviour. We investigated the relationship between the dynamics of the macroscopic ODEs and those of finite networks of oscillators and found that chaotic behaviour in the former does not necessarily bear any relationship to that in the latter. We briefly investigated the effects of adding temporal disorder in the form of Gaussian white noise to the oscillator dynamics and found that this could also result in new types of behaviour (not just "washing

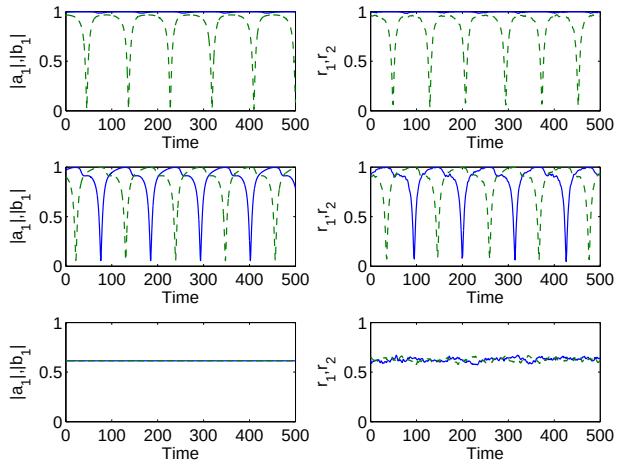

FIG. 11: Left column: $|a_1(t)|$ (solid) and $|b_1(t)|$ (dashed) from numerically solving (20)-(21) for $\sigma = 0.00003$ (top), $\sigma = 0.0003$ (middle) and $\sigma = 0.01$ (bottom). Right column: $r_1(t)$ (solid) and $r_2(t)$ (dashed), where $r_1 = |(1/1000)\sum_{j=1}^{1000}\exp(i\theta_j)|$ and $r_2 = |(1/1000)\sum_{j=1001}^{2000}\exp(i\theta_j)|$, for the same noise intensities as in the left column. Parameters: $D = 0, \alpha = \pi/2 - 0.05, A = 0.37$.

out" of dynamics).

It is known that networks of identical, sinusoidally coupled phase oscillators have non-generic behaviour [48], and that making them non-identical reduces the number of variables needed for their macroscopic description [16]. We have shown here that increasing the amount of disorder in the network by making the oscillators more and more heterogeneous in a simple systematic way can lead to fundamentally new behaviour, going against the intuition that increasing disorder can only destroy, rather than create, non-trivial dynamics.

Acknowledgements: I thank the referees for their useful comments which helped improve the manuscript.

[1] S. Camazine, J. Deneubourg, N. Franks, J. Sneyd, G. Theraula, and E. Bonabeau, *Self-Organization in Biological Systems* (Princeton University Press, 2003).
[2] A. Pikovsky, M. Rosenblum, and J. Kurths, *Synchronization* (Cambridge U. Press, Cambridge, U. K., 2003).
[3] A. T. Winfree, *The Geometry of Biological Time* (Springer, New York, 1980).
[4] O. V. Popovych, Y. L. Maistrenko, and P. A. Tass, Phys. Rev. E **71**, 065201 (2005).
[5] C. Baesens, J. Guckenheimer, S. Kim, and R. MacKay, Physica D **49**, 387 (1991).
[6] P. Matthews, R. Mirollo, and S. Strogatz, Physica D **52**, 293 (1991).
[7] S. Strogatz and R. Mirollo, Journal of Statistical Physics **63**, 613 (1991).
[8] S. Strogatz, Physica D **143**, 1 (2000).
[9] D. Abrams, R. Mirollo, S. Strogatz, and D. Wiley, Phys. Rev. Lett. **101**, 084103 (2008).
[10] C. R. Laing, Physica D **238**, 1569 (2009).
[11] J. Acebrón, L. Bonilla, C. Pérez Vicente, F. Ritort, and R. Spigler, Rev. Mod. Phys. **77**, 137 (2005).
[12] N. Balmforth and R. Sassi, Physica D: Nonlinear Phenomena **143**, 21 (2000).
[13] M. Wolfrum, O. E. Omel'chenko, S. Yanchuk, and Y. L. Maistrenko, Chaos **21**, 013112 (2011).
[14] C. Bick, M. Timme, D. Paulikat, D. Rathlev, and P. Ashwin, Phys. Rev. Lett. **107**, 244101 (2011).
[15] P. So and E. Barreto, Chaos **21**, 033127 (pages 11) (2011).
[16] E. Ott, B. R. Hunt, and T. M. Antonsen, Chaos **21**, 025112 (2011).
[17] E. Ott and T. M. Antonsen, Chaos **19**, 023117 (2009).
[18] E. Ott and T. M. Antonsen, Chaos **18**, 037113 (2008).
[19] E. A. Martens, E. Barreto, S. H. Strogatz, E. Ott, P. So, and T. M. Antonsen, Phys. Rev. E **79**, 026204 (2009).
[20] B. Luce, Physica D: Nonlinear Phenomena **84**, 553 (1995).
[21] S. Wiggins, *Introduction to Applied Nonlinear Dynamical Systems and Chaos*, vol. 2 (Springer Verlag, 2003).
[22] C. Sparrow, *The Lorenz Equations: Bifurcations, Chaos, and Strange Attractors*, vol. 41 (Springer Verlag, 1982).
[23] C. R. Laing, Chaos **19**, 013113 (2009).
[24] E. Montbrió, J. Kurths, and B. Blasius, Phys. Rev. E **70**, 056125 (2004).
[25] E. Barreto, B. Hunt, E. Ott, and P. So, Phys. Rev. E **77**, 036107 (2008).
[26] P. Skardal and J. Restrepo, Physical Review E **85**, 016208 (2012).
[27] D. Abrams and S. Strogatz, Phys. Rev. Lett. **93**, 174102 (2004).
[28] D. Abrams and S. Strogatz, Int. J. Bifurcat. Chaos **16**, 21 (2006).
[29] S. Shima and Y. Kuramoto, Phys. Rev. E **69**, 036213 (2004).
[30] M. Tinsley, S. Nkomo, and K. Showalter, Nature Physics (2012).
[31] K. Wiesenfeld, P. Colet, and S. H. Strogatz, Phys. Rev. E **57**, 1563 (1998).
[32] F. Dörfler and F. Bullo, SIAM Journal on Control and Optimization **50**, 1616 (2012).
[33] A. Hagerstrom, T. Murphy, R. Roy, P. Hövel, I. Omelchenko, and E. Schöll, Nature Physics (2012).
[34] E. A. Martens, Phys. Rev. E **82**, 016216 (2010).
[35] C. R. Laing, Physica D: Nonlinear Phenomena **240**, 1960 (2011).
[36] E. Montbrió and D. Pazó, Phys. Rev. Lett. **106**, 254101

(2011).
[37] P. S. Skardal, E. Ott, and J. G. Restrepo, Phys. Rev. E **84**, 036208 (2011).
[38] L. M. Alonso and G. B. Mindlin, Chaos **21**, 023102 (pages 5) (2011).
[39] W. S. Lee, J. G. Restrepo, E. Ott, and T. M. Antonsen, Chaos **21**, 023122 (pages 14) (2011).
[40] S. A. Marvel and S. H. Strogatz, Chaos **19**, 013132 (pages 9) (2009).
[41] W. S. Lee, E. Ott, and T. M. Antonsen, Phys. Rev. Lett. **103**, 044101 (2009).
[42] H. Hong and S. H. Strogatz, Phys. Rev. Lett. **106**, 054102 (2011).
[43] L. M. Childs and S. H. Strogatz, Chaos **18**, 043128 (pages 9) (2008).
[44] G. Barlev, T. M. Antonsen, and E. Ott, Chaos **21**, 025103 (2011).
[45] C. R. Laing, K. Rajendran, and I. G. Kevrekidis, Chaos **22**, 013132 (2012).
[46] Y. Kuramoto, *Chemical Oscillations, Waves, and Turbulence* (Springer, Berlin, 1984).
[47] MATLAB, *version 7.13.0.564 (R2011b)* (The MathWorks Inc., Natick, Massachusetts, 2011).
[48] S. Watanabe and S. Strogatz, Physica D **74**, 197 (1994).
[49] A. Pikovsky and M. Rosenblum, Phys. Rev. Lett. **101**, 264103 (2008).
[50] G. Demeter and L. Kramer, Phys. Rev. Lett. **83**, 4744 (1999).
[51] B. Deng, SIAM J. Math. Anal. **21**, 693 (1990).
[52] Y. Kuznetsov, *Elements of Applied Bifurcation Theory*, vol. 112 (Springer Verlag, 1995).
[53] J. M. Greene and J.-S. Kim, Physica D: Nonlinear Phenomena **24**, 213 (1987).
[54] C. Laing and G. J. Lord, eds., *Stochastic Methods in Neuroscience* (OUP Oxford, 2009), pp. 1–28.
[55] G. Ermentrout and D. Terman, *Mathematical Foundations of Neuroscience*, vol. 35 (Springer Verlag, 2010).